PNAS RESEARCH ARTICLE | ENGINEERING PHARMACOLOGY

Immune-infiltrated kidney organoid-on-chip model for assessing T cell bispecific antibodies

Katharina T. Kroll[a,b,1], Mariana M. Mata[a,b,1], Kimberly A. Homan[a,b,c,2], Virginie Micallef[d], Alejandro Carpy[e], Ken Hiratsuka[f,g], Ryuji Morizane[f,g], Annie Moisan[d], Marcel Gubler[d], Antje-Christine Walz[d], Estelle Marrer-Berger[d], and Jennifer A. Lewis[a,b,2]

Contributed by Jennifer A. Lewis; received April 4, 2023; accepted July 10, 2023; reviewed by Peter Loskill and Kyle McCracken

T cell bispecific antibodies (TCBs) are the focus of intense development for cancer immunotherapy. Recently, peptide-MHC (major histocompatibility complex)-targeted TCBs have emerged as a new class of biotherapeutics with improved specificity. These TCBs simultaneously bind to target peptides presented by the polymorphic, species-specific MHC encoded by the human leukocyte antigen (HLA) allele present on target cells and to the CD3 coreceptor expressed by human T lymphocytes. Unfortunately, traditional models for assessing their effects on human tissues often lack predictive capability, particularly for "on-target, off-tumor" interactions. Here, we report an immune-infiltrated, kidney organoid-on-chip model in which peripheral blood mononuclear cells (PBMCs) along with nontargeting (control) or targeting TCB-based tool compounds are circulated under flow. The target consists of the RMF peptide derived from the intracellular tumor antigen Wilms' tumor 1 (WT1) presented on HLA-A2 via a bivalent T cell receptor-like binding domain. Using our model, we measured TCB-mediated CD8$^+$ T cell activation and killing of RMF-HLA-A2-presenting cells in the presence of PBMCs and multiple tool compounds. DP47, a non-pMHC-targeting TCB that only binds to CD3 (negative control), does not promote T cell activation and killing. Conversely, the nonspecific ESK1-like TCB (positive control) promotes CD8$^+$ T cell expansion accompanied by dose-dependent T cell–mediated killing of multiple cell types, while WT1-TCB* recognizing the RMF-HLA-A2 complex with high specificity, leads solely to selective killing of WT1-expressing cells within kidney organoids under flow. Our 3D kidney organoid model offers a platform for preclinical testing of cancer immunotherapies and investigating tissue-immune system interactions.

kidney organoids | organ-on-chip | T cell bispecific antibodies | immuno-oncology

T cell bispecific antibodies (TCBs) are an emerging class of immuno-oncology drugs that selectively recruit T cells to tumor cells (1, 2). Among them are T cell receptor-like TCBs, which target peptide-major histocompatibility complex I (MHCI) complexes. They contain two moieties, one that targets a tumor-associated antigen presented by MHCI and another that binds to the invariant chain of the T cell receptor, CD3. By facilitating binding of cytotoxic CD8$^+$ T cells to cancer cells, TCBs elicit T cell–mediated cell killing against the targeted cells via release of cytotoxic granules that contain perforins and granzymes (1, 3, 4). One target of substantial interest is Wilms Tumor 1 (WT1), a highly validated tumor antigen that is overexpressed in multiple leukemias and solid tumors (5–7). To effectively target intracellular antigens, one must develop TCBs that bind to human leukocyte antigen (HLA) presented peptides. For WT1, several epitopes have been identified, including $WT1_{126–134}$ (RMFPNAPYL, commonly referred to as RMF) presented on HLA-A*02:01 (HLA-A2) (3, 4, 8, 9).

A concomitant challenge for cancer immunotherapy is the development of human model systems that recapitulate the requisite tissue cell diversity, 3 dimensional architecture, and physiological function needed to evaluate pharmacological and toxicological effects of these complex molecules. It is well known that WT1 is expressed in podocytes in adult kidneys (5, 10, 11); however, relevant kidney models for assessing a potential "on-target, off-tumor" effect of these RMF-HLA-A2 targeted TCBs are lacking. For example, humanized mouse models have limited utility due to their distinct differences in immune response and tissue-specific HLA I immunopeptidomes (12–14). While the use of 2 dimensional cell culture models based on primary or immortalized adult podocytes is limited either by lack of cell proliferation leading to a scalability challenge or proper gene expression that may jeopardize predictivity (15, 16). More sophisticated 2 dimensional models, e.g., glomerulus-on-chip models, have recently been introduced, which contain podocytes derived from human induced pluripotent stem cells and endothelial cells assembled into monolayers on the top and bottom surfaces of a porous membrane within a microfluidic chip and subjected to flow (17, 18). While those models have potential utility, they have not yet been used for profiling of these

Significance

Human models that recapitulate the cellular diversity, 3 dimensional architecture, and physiological function of native tissues are needed to evaluate emerging cancer immunotherapeutics, such as T cell bispecific antibodies (TCBs). One target of substantial interest is Wilms Tumor 1 (WT1), a highly validated tumor antigen expressed in multiple leukemias and solid tumors as well as podocytes present in human kidneys. To assess their "off-tumor, on-target" effects, we created an immune-infiltrated, vascularized kidney organoid-on-chip model in which TCBs and peripheral blood mononuclear cells (PBMCs) are cocirculated. Using this model, we observed rapid CD8$^+$ T cell expansion and activation under flow accompanied by dose-dependent and selective T cell–mediated killing.

Competing interest statement: Trestle Biotherapeutics was not involved in this research but has licensed research in engineering kidney tissue for therapeutic use from Harvard University. R.M. and J.A.L. are members of the Trestle Biotherapeutics Scientific Advisory Board and received stock options. V.M., A.C., and M.G. are employed by Hoffmann-La Roche, Ltd. K.A.H. is currently employed by Genentech, but carried out this work as a postdoctoral researcher in the lab of J.A.L. A patent was filed on the vascularized kidney organoid-on-chip model, which was licensed by Harvard University to Trestle Biotherapeutics (startup company in San Diego, CA).

[1]K.T.K. and M.M.M. contributed equally to this work.

[2]To whom correspondence may be addressed. Email: homank@gene.com or jalewis@seas.harvard.edu.

This article contains supporting information online at https://www.pnas.org/lookup/suppl/doi:10.1073/pnas.2305322120/-/DCSupplemental.

Published August 21, 2023.

TCBs. Importantly, none of these models recapitulates the 3D microenvironment present within human kidneys, which are replete with podocyte-rich glomeruli, proximal and distal tubules, and microvascular networks that comprise their functional nephrons (19–21). Recapitulating different kidney epithelial and endothelial cell types in vitro is important since they can be exposed to TCBs in vivo (22, 23).

Here, we report an immune-infiltrated kidney organoid-on-chip model created by first differentiating human pluripotent stem cells (24, 25), then seeding these organoids on an adherent extracellular matrix (ECM), followed by circulating peripheral blood mononuclear cells (PBMCs) along with either nontargeting (control) or targeting TCBs under flow (Fig. 1*A*) (26). Three tool compounds are evaluated: 1) DP47, a negative control, that only binds to CD3, 2) ESK1-like TCB (3, 4), a nonselective HLA-A2-WT1 TCB used as a positive control, and 3) WT1-TCB* recognizing specifically the RMF-HLA-A2 complex reported in an earlier study by Augsberger et al. (Fig. 1*B*) (9). We note that the ESK1-like TCB is an earlier version of the latter molecule, which has been subsequently refined. Due to its lack of specificity (27), we expect the ESK1-like TCB to exhibit reactivity to HLA-A2-positive cells with low specificity for the presented peptide. WT1-TCB* was developed to increase specificity to the RMF-peptide. We first show that our kidney organoid model exhibits the desired HLA-A2 expression and can be cocultured with PBMCs from healthy individuals with minimal alloreactivity. As expected, DP47 (negative control) does not promote T cell activation and killing in the presence of PBMCs. However, when the ESK1-like TCB (positive control) is cocirculated with PBMCs, we find distinct differences in $CD8^+$ T cell expansion and activation markers under flow accompanied by dose-dependent T cell–mediated killing of multiple cell types. Finally, when the targeting WT1-TCB* is cocirculated, we only observe selective killing of WT1-expressing cells within the kidney organoids.

Results

Immune-Infiltrated Kidney Organoid-On-Chip Model. We created our kidney organoid-on-chip model by first seeding organoids onto an adherent gelatin–fibrin matrix on day 11/12 of their differentiation and cultured under low flow (~0.0001 dyn/cm^2) for approximately 12 h prior to the introduction of high flow (0.008 to 0.035 dyn/cm^2) conditions for 7 d (i.e., day 18/19 of their differentiation). As demonstrated previously, kidney organoids subjected to flow exhibit enhanced in vitro vascularization and maturation of both glomerular and tubular compartments (26). To determine whether our model fulfills the key prerequisites for TCB binding (4, 9), we first confirmed that cells within our kidney organoids express HLA-A2, which is necessary for presenting the $WT1_{RMF}$ peptide (*SI Appendix*, Table S1). We find that roughly 30% of these cells express HLA-A2 in the kidney organoids on chip, and importantly, this value increases above 80% when they are exposed to 500 U/mL of interferon γ (IFNγ), a proinflammatory signal known to induce upregulation of MHCI, for 3 d (28) (Fig. 1*C*, *SI Appendix*, Fig. S1*A*). Next, we characterized WT1 expression in our kidney organoid-based model using immunofluorescent staining on day 21 of differentiation (Fig. 1*D* and *SI Appendix*, Fig. S1*B*). We observed a high expression of WT1 in $PODXL^+$ podocyte clusters along with a lower expression in $actin^+$ stromal-like cells in the interstitium between the nephron epithelia. By contrast, LTL^+ proximal tubules, $CDH1^+$ distal tubules, and $CD31^+$ endothelial cells appeared negative for WT1. Our observations are in good agreement with a recently published single-cell RNA sequencing dataset generated for kidney organoids produced by the same protocol at day 26 of differentiation (*SI Appendix*, Fig. S1 *C* and *D*), which show that WT1 is expressed in high levels in the cluster identified as podocytes and in lower levels in the mesenchyme and first segment of the proximal tubule (PT1) in kidney organoids compared to podocytes and mesangium in an adult kidney dataset (29–31).

Next, we introduced PBMCs to generate an immune-infiltrated kidney organoid-on-chip model, since the TCB mechanism of action requires the presence of $CD3^+$ immune effector cells. We find that PBMCs exhibit high viability with greater than 80% live $CD45^+$ cell population over a 5-d period of recirculating flow on chip, which is comparable to the cell viability observed in static controls (Fig. 1*E*). Using immunofluorescence staining coupled with live confocal imaging, we find that 3 d after their introduction on chip, PBMCs are located throughout the kidney organoids, including within their microvascular network (Fig. 1*F* and Movie S1). To qualitatively assess T cell–mediated cell killing in our model, we carried out three preliminary experiments. In the absence of TCBs or presence of the negative control, DP47 (1 μg/mL), we observed minimal cell killing, as indicated by $caspase^+$ cells stained with FAM FLICA dye (Fig. 1*G*). However, upon adding the positive control, ESK-1 like TCB, we observed a substantial increase in $caspase^+$ cells and infiltration of $CD8^+$ T cells (Fig. 1*G* and *SI Appendix*, Fig. S2) within the kidney organoids on chip.

Flow Effects on ESK1-Like TCB-Mediated Cytokine Release, Cell Expansion, and Killing. To investigate the effect of flow on cell killing, we carried out a series of experiments in which either no TCBs and no PBMCs (no PBMC), no TCB but PBMCs (no TCB), or both PBMCs and the ESK-1 like TCB (1 μg/mL) are circulated under low (~0.0001 dyn/cm^2) or high flow (0.008 to 0.035 dyn/cm^2) conditions (26). In the absence of PBMCs ($CD45^+$ population), we observed little difference between HLA-A2 expression in the live $CD45^-$ population within the kidney organoids with or without introducing the ESK1-like TCB on chip (Fig. 2*A*). We performed these experiments without exogenous IFNγ stimulation. By contrast, there is a substantial increase in HLA-A2 expression in the live $CD45^-$ population in the presence of PBMCs (no TCB). When PBMCs and the ESK1-like TCB are cocirculated, there is a twofold increase in HLA-A2 expression in the live $CD45^-$ population under low and high flow conditions at day 5. Concomitantly, the IFNγ concentration in the chip culture medium increases substantially over day 1 to day 5 when PBMCs and the ESK1-like TCB are cocirculated on chip (*SI Appendix*, Fig. S3*A*). Similar trends are observed for Interleukin 2 (IL-2) and Tumor Necrosis Factor α (TNFα) as well as Interleukin 8 (IL-8) and Interleukin 10 (IL-10) levels (*SI Appendix*, Fig. S3*A*) under the same conditions. Based on earlier findings (Fig. 1*C*), we attribute the upregulation of HLA-A2 in the kidney organoids predominantly to release of IFNγ. We further posit that the sharp increase in cytokine release observed over this 5-d period arises due to TCB-mediated cell expansion and killing.

To assess TCB-mediated cell expansion, we measured the cytotoxic $CD8^+$ T cell population within the $CD45^+$ PBMCs in the absence and presence of the ESK1-like TCB under low and high flow conditions on chip. The $CD8^+$ T cell population exhibits a twofold expansion in the presence of this TCB with negligible differences between the two flow conditions (Fig. 2*B*). However, their activation state measured by expression of CD69, an early activation marker (32, 33), CD25, a late activation marker (34, 35), and HLA-DR, an important marker for both activation and T cell receptor engagement (36), is influenced by flow (Fig. 2*C* and *SI Appendix*, Fig. S3*B*). Under high flow, we find a statistically significant increase in HLA-DR expression indicating

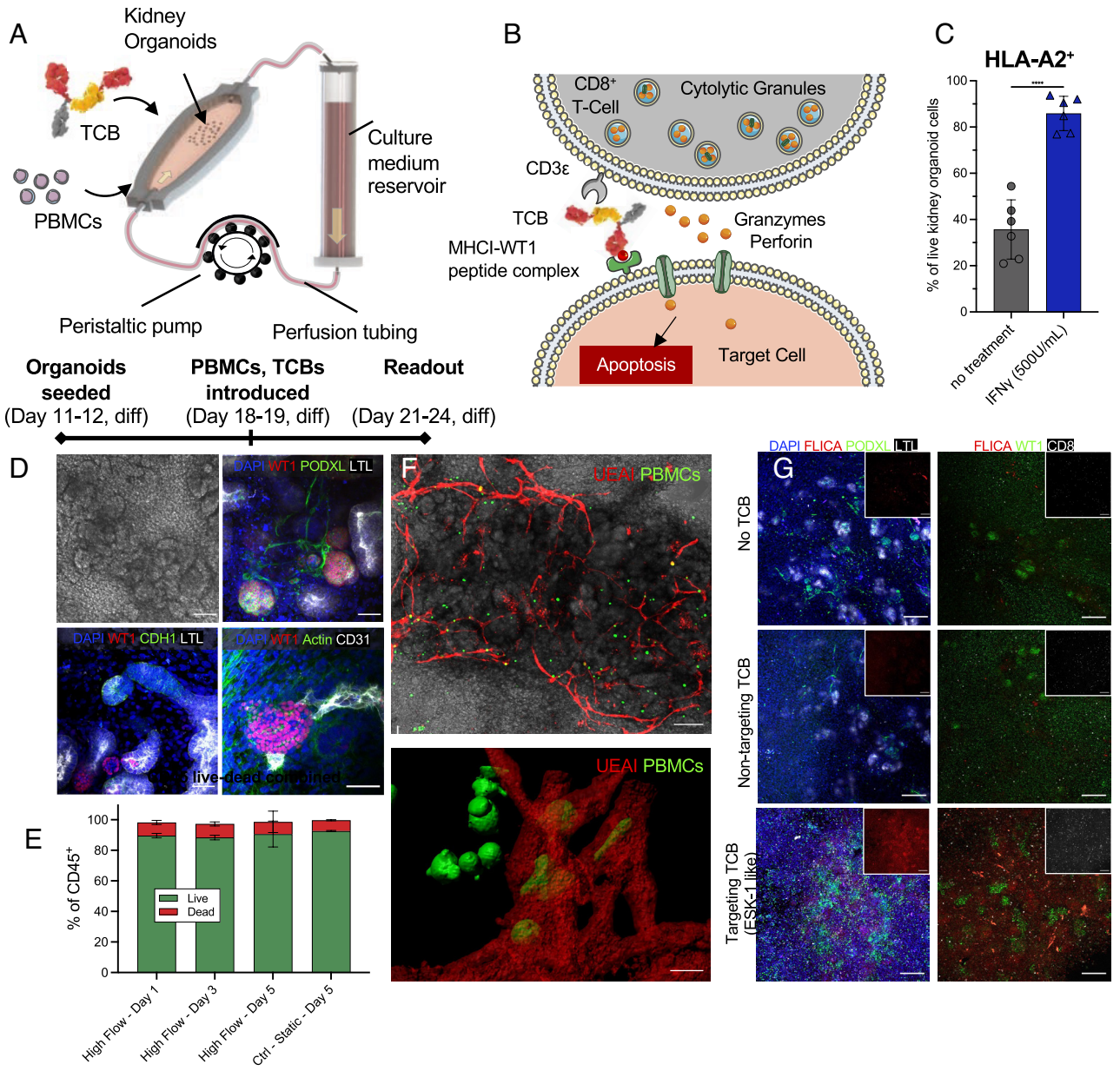

Fig. 1. Immune-infiltrated kidney organoid-on-chip model for assessing TCBs. (*A*) Schematic illustration of the experimental setup. Organoids are seeded onto the millifluidic chip device on their day 11/12 of differentiation and cultured for 7 d under high flow culture conditions. On day 18/19 of kidney organoid differentiation, PBMCs are seeded into the millifluidic chip chamber, the TCB is added to the reservoir, and the chip is cultured under high flow culture conditions for 3 to 5 d until the readout assay is performed. (*B*) Schematic illustration of the mechanism of action of the TCB antibody: The TCB targets the effector cell, a $CD8^+$ T cell to the cell of interest and the target cell is killed by release of cytolytic granules containing perforins and granzymes. (*C*) Human leukocyte antigen A2 (HLA-A2) expression quantified by flow cytometry analysis in kidney organoids cultured under high flow with (blue bars) or without (gray bars) 500 U/mL IFNγ for 3 d. **** indicates $P < 0.0001$ (*D*) Representative maximum intensity projections of confocal microscopy images showing the WT1 expression in the kidney organoids under high flow culture conditions in respect to the nephron structures of interest. The top left image in each panel is a representative bright-field image of the organoids structure, (scale bar for these grayscale images is 100 μm.) Podocalyxin (PODXL) labels podocytes, lotus tetranoglobus lectin (LTL) labels proximal tubules, E-Cadherin (CDH1) labels distal tubules, and Cluster of Differentiation 31 (CD31) labels endothelial cells. (Scale bar for the immunofluorescence images is 50 μm.) (*E*) Flow cytometry live/dead analysis of the $CD45^+$ PBMC population under high flow compared to PBMCs in a static dish without organoids (Ctrl–Static). (*F*) Representative maximum intensity projections of confocal microscopy live images showing the PBMCs (labeled by CellMask™ Green) and the vasculature labeled by UEAI (red) in the kidney organoids under flow (upper image). The lower images show a 3D rendering of the same samples from a higher magnification image (*G*) Representative maximum intensity projections of confocal microscopy images showing the effect of adding TCBs and PBMCs to kidney organoids under high flow on chip. The kidney organoids in these conditions were cultured in the presence of either no TCB, a nontargeting TCB (DP47), or a targeting TCB (ESK1-like). The samples are stained for either nuclei (DAPI, blue), active caspases (FLICA, red), podocytes (PODXL, green), and proximal tubules (LTL, gray), or active caspases (FLICA, red), Wilms Tumor 1 (WT1, green), and cluster of differentiation (CD8, gray). The insets show either only the active caspases (FLICA, red) or the CD8 infiltration (CD8, gray). (Scale bars are 200 μm.)

potentially higher $CD8^+$ T cell activation. These observations are in good agreement with recent experiments exploring the effects of shear stress on T cells (37, 38). Based on these data, we anticipated that higher T cell–mediated killing would occur for kidney organoids on chip under high flow. To investigate TCB-mediated cell killing, we characterized the live/dead $CD45^-$ cell population as well as LDH (lactate dehydrogenase) release for the four experimental conditions studied for the ESK1-like TCB on chip. There was a 2.5-fold increase in dead $CD45^-$ cells isolated from the kidney organoids (and PBMCs) when we carried out the cytotoxicity assay under high flow conditions for 5 d (Fig. 2*D*). However, when kidney organoids are subjected to low flow on chip, there

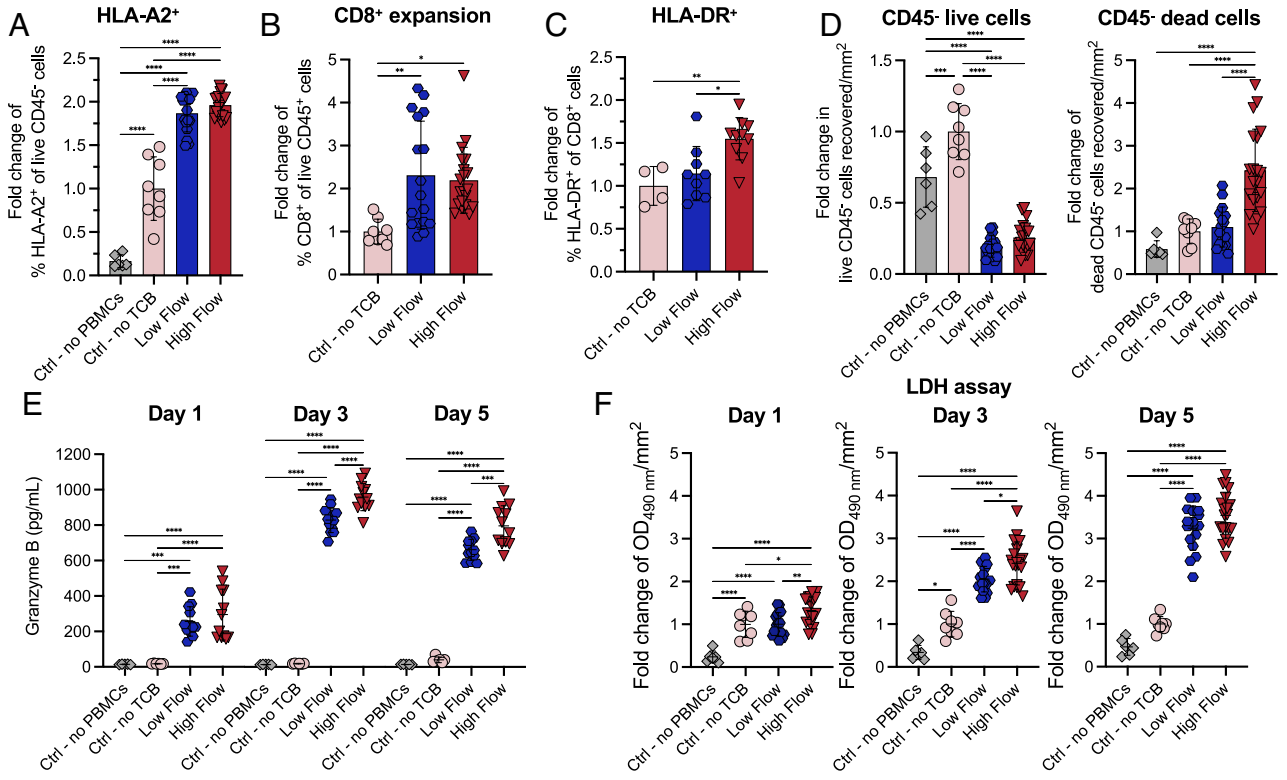

Fig. 2. Flow effects on ESK1-like TCB–mediated cell expansion and killing. (*A*) Fold change of %HLA-A2$^+$ in the CD45$^-$ population analyzed by flow cytometry in the respective culture condition. Data are expressed as a fold change compared to Ctrl–no TCB and are normalized by the organoid area 1 d after seeding. Control samples and the "High Flow" condition are cultured under high flow; the "Low Flow" condition is cultured under low flow conditions. Control samples without the TCB, low flow, and high flow samples are culture with PBMCs, and low flow and high flow samples are cultured with PBMCs and TCBs. (*B*) Fold change of %CD8$^+$ in the live CD45$^+$ population in the respective culture condition. (*C*) Fold change of %HLA-DR+ in the CD8$^+$ population (from *B*) in the respective culture condition. (*D*) Fold change in the live and dead CD45$^-$ negative cells compared to Ctrl–no TCB in the indicated culture conditions normalized by the organoid area 1 d after seeding. (*E*) Luminex assay data detecting Granzyme B in the culture medium supernatant of the respective culture condition. (*F*) LDH assay data of the TCB and T cell–mediated cell killing assay in the respective culture condition. (*A–D* and *F*) Fold change is normalized to the no TCB condition in each experiment to account for differences between donors. Asterisks indicate *P*-values in the one-way ANOVA with Tukey's post-test as follows: **P* < 0.0332, ***P* < 0.0021, ****P* < 0.0002, *****P* < 0.0001.

was no statistically significant difference in dead CD45$^-$ cells compared to the no TCB control. Furthermore, when we analyzed the supernatant for Granzyme B, we find substantially higher amounts under high flow (Fig. 2*E*) supporting our expectation of higher cell death under these conditions. To further quantify cell killing, we measured LDH released from the kidney organoids on day 1, 3 and 5, which is present in the circulating media on chip (Fig. 2*F*). We observed a modest increase in baseline LDH release in the presence of PBMCs (no TCB). While kidney organoids exposed to both PBMCs and the ESK1-like TCB on chip showed statistically significantly higher LDH release under both low and high flow conditions. Taken together, we find specific differences in CD8$^+$ T cell activation under high and low flow with an increased T cell–mediated killing of kidney organoid cells under high flow.

Dose-Dependent Response of ESK1-Like TCB. Using our immune-infiltrated kidney organoid-on-chip model, we assessed the dose-dependent response of the ESK1-like TCB. We focused on concentration ranges from 1 to 10 μg/mL for DP47 (negative control) and 0 to 1 μg/mL for the ESK1-like TCB. We first investigated the expression of HLA-A2 in the live CD45$^-$ population in response to the increasing stimulation with the two TCBs under high flow (Fig. 3*A*). While HLA-A2 expression increased in the presence of DP47 compared to the no PBMC control, there was no statistically significant difference relative to control without DP47, but with PBMCs. Using the ESK1-like TCB, we observed a dose-dependent increase in HLA-A2 expression that plateaued at 0.1 μg/mL. Concomitantly, a dose-dependent increase of IFNγ is observed in the perfusate in the presence of the ESK1-like TCB (Fig. 3*B*). Similarly, we observed highest levels of IFNγ, IL-2, TNFα, IL-10, and IL-8 in the perfusate from kidney organoid-on-chip models exposed to 1 μg/mL ESK1-like TCB under flow (Fig. 3*B* and *SI Appendix*, Fig. S4 *A* and *B*). Regarding T cell expansion and activation, we find that DP47 did not lead to a statistically significant increase in CD8$^+$ cells compared to control, while cytolytic T cells in the CD45$^+$ cell population appeared to expand in a dose-dependent manner in the presence of the ESK1-like TCB (Fig. 3*C*). In their activation state, samples exposed to DP47 did not exhibit statistically significant differences compared to the no TCB control. While no dose dependency in the activation state was detected, we did find that CD69, CD25, and HLA-DR surface expression are highest for models exposed to 1 μg/mL ESK1-like TCB (Fig. 3*D* and *SI Appendix*, Fig. S4 *C* and *D*).

To quantify T cell–mediated cell killing, we analyzed the renal epithelial structure, live/dead CD45$^-$ cell population, and LDH release from our kidney organoid on the chip model. Using bright-field microscopy, we find that the organoid structure is unaffected solely by PBMCs, but it degraded substantially in the presence of the ESK1-like TCB (1 μg/mL) (Fig. 3*E*). CD8$^+$PRF1$^+$ T cells are observed to be in close proximity to kidney organoid cells at day 3 under the same conditions (Fig. 3*F*). To confirm these results, we quantified the live and dead CD45$^-$ kidney organoid cell populations by flow cytometry (Fig. 3*G*). The

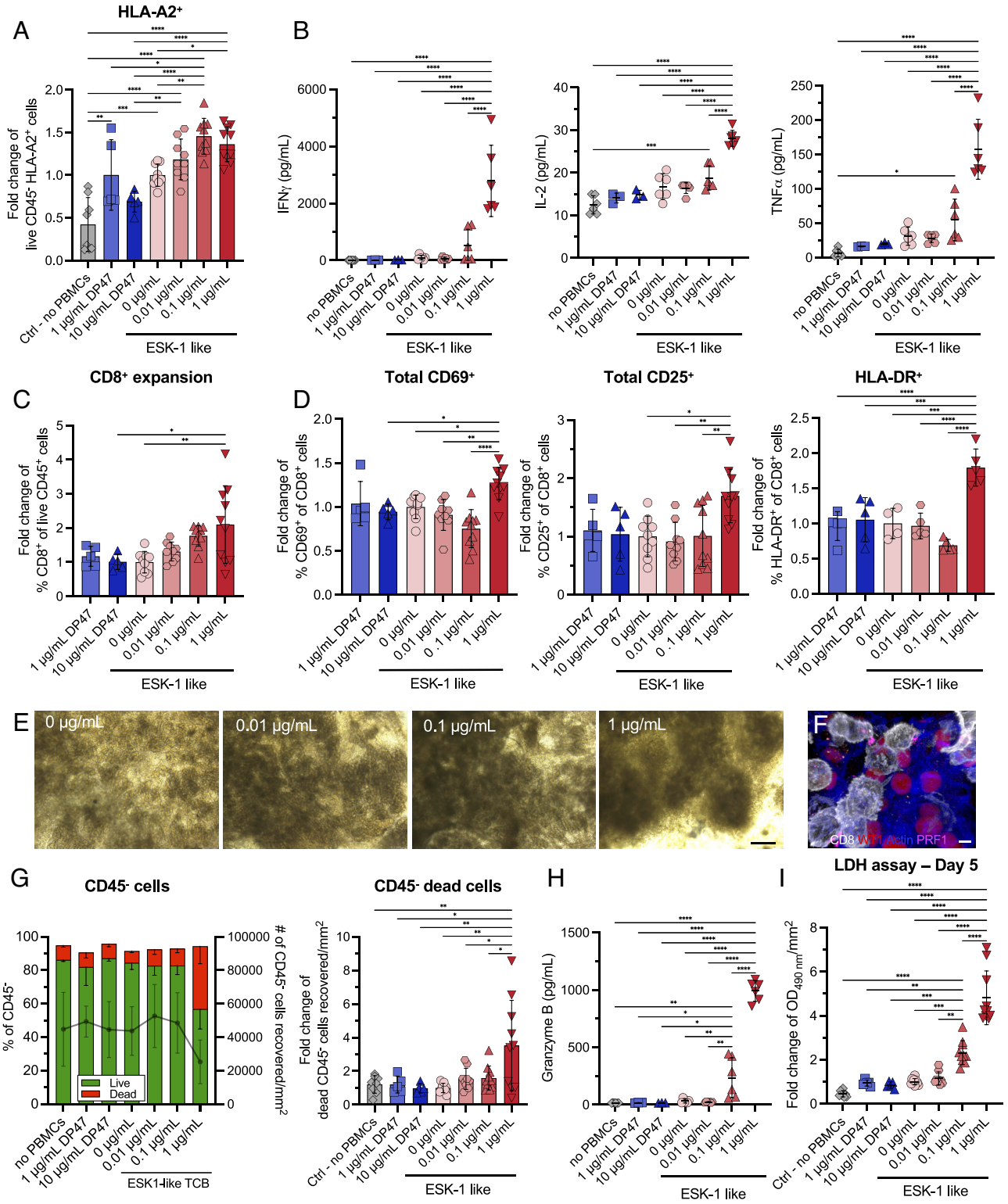

Fig. 3. Dose-dependent response of ESK1-like TCB–mediated cell killing. (*A*) Fold change of %HLA-A2$^+$ in the CD45$^-$ population exposed to either DP47 or ESK1-like TCB in the indicated concentration. (*B*) Luminex assay data on day 5 for IFNγ, IL-2, and TNFα in the respective culture condition. (*C*) Fold change of %CD8$^+$ in the live CD45$^+$ population in the respective culture condition. (*D*) Fold change of %CD69$^+$, %CD25$^+$, and %HLA-DR+ in the CD8$^+$ population (from *G*) exposed to either DP47 or ESK1-like TCB in the indicated concentration. The Ctrl–no PBMC control is omitted, since those samples are not seeded with CD45$^+$ cells. (*E*) Representative bright-field images on day 5 of the TCB-mediated cytotoxicity assay with the TCB concentration indicated on the image (white). (Scale bar is 500 µm.) (*F*) Representative 3D reconstruction of a confocal microscopy image showing CD8$^+$ PRF1$^+$ T cells (gray, magenta) near WT1$^+$ Actin$^+$ organoid cells. (Scale bar is 5 µm.) (*G*) *Left*: % live/dead cells in the CD45$^-$ population plotted in solid bars on the left *y* axis and total number of CD45$^-$ cells recovered from the sample plotted as dots on the right *y* axis exposed to either DP47 or ESK1-like TCB in the indicated concentration. *Right*: Fold change of the dead CD45$^-$ negative cells compared to Ctrl–no TCB in the indicated culture conditions normalized by the organoid area 1 d after seeding. (*H*) Luminex assay data on day 5 for Granzyme B in the respective culture condition. (*I*) LDH assay data for day 5 of the TCB cytotoxicity assay. Data are expressed as a fold change compared to Ctrl–no TCB and is normalized by the organoid area 1 d after seeding. (*A*, *C*, *D*, *G*, and *I*) Fold change is normalized to the no TCB condition in each experiment to account for differences between donors. Asterisks indicate *P*-values in the one-way ANOVA with Tukey's post-test as follows: *$P < 0.0332$, **$P < 0.0021$, ***$P < 0.0002$, ****$P < 0.0001$.

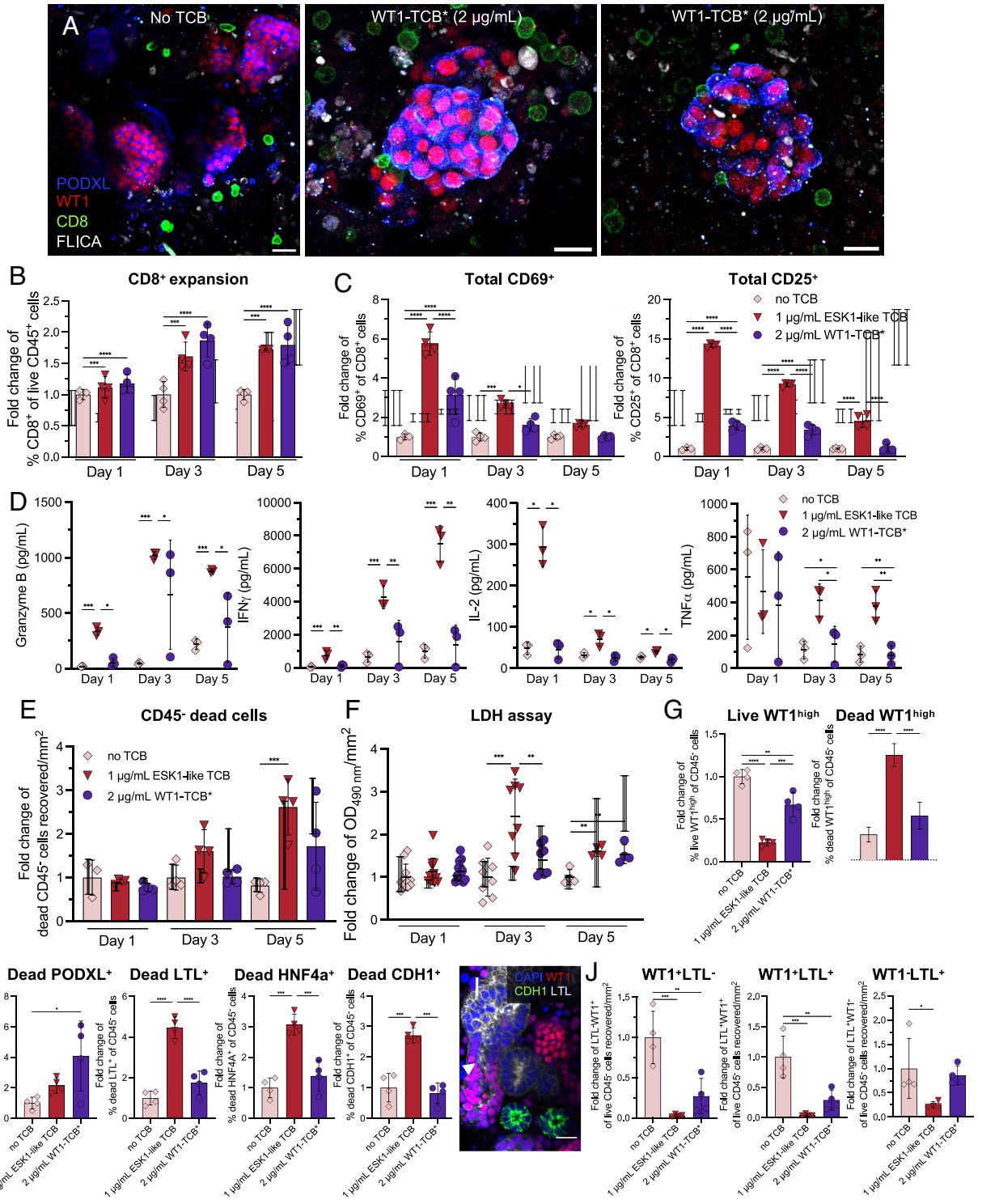

Fig. 4. Target specificity of WT1-TCB*-mediated cell killing. (*A*) Representative maximum intensity projections of confocal microscopy images of the kidney organoids on day 4 of the TCB-mediated cytotoxicity assay (from Z-stack videos in Movie S3). The samples were either cultured without (*Left*) or with the addition of 2 µg/mL WT1-TCB* (*Right*) and stained for active caspases (FLICA, gray), nuclei (DAPI, blue), CD8 T cells (CD8, green), and podocytes (PODXL, blue). (Scale bar is 20 µm.) (*B*) Expansion of $CD8^+$ T cells in the live $CD45^+$ population exposed to either ESK1-like TCB or WT1-TCB* in the indicated concentration (plot legend shown in (C)). (*C*) Fold change of $\%CD69^+$, and $\%CD25^+$ in the $CD8^+$ population (from *D*) exposed to either ESK1-like TCB or WT1-TCB* in the indicated concentration. (*D*) Luminex assay data for Granzyme B, IFNγ, IL-2, and TNFα in the respective culture condition. (*E*) Fold change in the dead $CD45^-$ negative cells compared to Ctrl–no TCB in the indicated culture conditions normalized by the organoid area 1 d after seeding. (*F*) LDH assay data for days 1, 3, and 5 of the TCB cytotoxicity assay. Data are expressed as a fold change compared to Ctrl–no TCB and is normalized by the organoid area 1 d after seeding. (*G*) Proportion of the $WT1^{high}$ expressing cell populations either live (*Left*) or dead (*Right*) in the $CD45^-$ cell population exposed to either ESK1-like TCB or WT1-TCB* in the indicated concentration. (*H*) Proportion of the dead $PODXL^+$, dead LTL^+, dead $HNF4A^+$, and dead $CDH1^+$ cell populations in the $CD45^-$ cell population exposed to either ESK1-like TCB or WT1-TCB* in the indicated concentration. (*I*) Representative maximum intensity projections of confocal microscopy images of the kidney organoids on day 21 of differentiation cultured in static conditions showing WT1 (red) cells, proximal tubule cells (LTL, gray), nuclei (DAPI, blue), and distal tubule cells (CDH1, green). The white arrows indicate $WT1^+LTL^+$ cells. (Scale bar is 20 µm.) (*J*) Number of cells recovered from the live CD45- population that are either WT1 single positive (*Left*), WT1 and LTL double positive (*Middle*), or LTL single positive (*Right*). The samples are exposed to either ESK1-like TCB or WT1-TCB* in the indicated concentration. The number of cells is normalized by the organoid area 1 d after seeding. (*B*, *E–H*, and *J*) Fold change is normalized to the no TCB condition. Asterisks indicate *P*-values in the one-way ANOVA with Tukey's post-test as follows: $*P < 0.0332$, $**P < 0.0021$, $***P < 0.0002$, $****P < 0.0001$.

presence of PBMCs alone did not alter the live/dead $CD45^-$ population, nor did the presence of DP47. However, there is a statistically significant decrease in live $CD45^-$ cells in the presence of 1 μg/mL ESK1-like TCB. The fraction of dead $CD45^-$ cells increased modestly at lower ESK1-like TCB concentrations compared to the no TCB control. Notably, the observed population of dead $CD45^-$ cells is statistically significant at a dose of 1 μg/mL ESK1-like TCB. Concomitantly, we also find a dose-dependent increase in Granzyme B in the supernatant (Fig. 3*H* and *SI Appendix*, Fig. S4*E*). Last, we carried out an LDH assay (Fig. 3*I* and *SI Appendix*, Fig. S4*F*), which, on day 5, revealed no increase in LDH signal in the presence of DP47 TCB but a dose-dependent increase of LDH signal beginning at 0.1 μg/mL ESK1-like TCB. Taken together, these observations support the use of our 3D model for dose-dependent studies.

Target Specificity of WT1-TCB*. To further assess target specificity, we carried out a series of experiments that compared T cell–mediated cell killing in our immune-infiltrated model in the presence of ESK1-like TCB (1 μg/mL) or WT1-TCB* (2 μg/mL) on days 1, 3, and 5 under high flow conditions (9, 39, 40). Using a labeled WT1-TCB*, we find that this compound has a high affinity for podocyte-rich clusters in the kidney organoid-on-chip model with or without exogenous IFNγ stimulation (Movie S2). Next, using a caspase reporter, we qualitatively observed a modest increase in FLICA signal with a marked increase in $CD8^+$ T cells and deterioration of podocyte clusters in the presence of WT1-TCB*, compared to the control (no TCB) (Fig. 4*A*, *SI Appendix*, Fig. S5*A*, and Movie S3). To quantify these effects, we carried out a series of experiments in which either no TCB, an ESK1-like TCB (1 μg/mL), or the WT1-TCB* (2 μg/mL) are cocirculated with PBMCs in our kidney organoid-on-chip model under high flow. Compared to the no TCB control, flow cytometry $CD8^+$ T cell data revealed a significant expansion of the $CD8^+$ population in the presence of either TCB at days 3 and 5 (Fig. 4*B*). In their activation state, ESK1-like TCB elicited robust CD69 expression from day 1 to 5, while WT1-TCB* induced this response to a lesser extent over the same period. (Fig. 4*C* and *SI Appendix*, Fig. S5*B*). By contrast, the expression of CD25, a late activation marker, first increased up to day 3, followed by a marked decrease for both TCBs by day 5. Importantly, while ESK1-like TCB induces a strong cytokine release (i.e., Granzyme B, IFNγ, IL-2, TNFα, IL-10, and IL-8), this is not observed in the presence of WT1-TCB* (Fig. 4*D* and *SI Appendix*, Fig. S5*C*). To investigate WT1-TCB*-mediated cell killing, we first analyzed the live/dead $CD45^-$ population. By day 5, there is a marked increase in the dead $CD45^-$ population in the presence of ESK1-like TCB (Fig. 4*E* and *SI Appendix*, Fig. S5*D*), while WT1-TCB* induced less cell killing over the 5-d period (Fig. 4*E* and *SI Appendix*, Fig. S5*E*) in good agreement with the LDH release data (Fig. 4*F*). Concomitantly, Granzyme B increased in the presence of both TCBs, but only the ESK1-like TCB is significantly higher than the no TCB control (Fig. 4*D*).

To further explore TCB-mediated cell killing, we focused on cells with high WT1 ($WT1^{high}$) expression. Immunofluorescent staining suggests that WT1 is more strongly expressed in podocytes (Figs. 1*D* and 4*G* and *SI Appendix*, Fig. S5*F*), which exhibited an increase in cell death in the presence of both ESK1-like TCB and the WT1-TCB*. Hence, we divided these cells into key subpopulations: $PODXL^+$ podocytes, LTL^+ and $HNF4a^+$ proximal tubule epithelial cells, and $CDH1^+$ distal tubule epithelial cells. Each of these cells experienced TCB-mediated cell killing in the presence of ESK1-like TCB, while preferential killing of podocytes is observed in the presence of WT1-TCB* compared to the control (no TCB) (Fig. 4*H*). To understand why WT1-TCB* led to modest killing of LTL^+ cells, we used confocal microscopy to reveal the presence of a small subpopulation of $WT1^+$-LTL^+ cells that reside in the transition region between the developing glomeruli and proximal tubules (Fig. 4*I*). While all $WT1^+LTL^-$, $WT1^+LTL^+$, and $WT1^-LTL^+$ cells are killed by the ESK1-like TCB, only the $WT1^+$ cells are killed by WT1-TCB* further highlighting its selectivity toward cells expressing WT1 and with the potential to present a WT1-derived peptide in a complex with HLA-A2 (Fig. 4*J*).

Discussion

To address the growing need for human model systems of high predictivity for immuno-oncology (15, 41), we created an immune-infiltrated kidney organoid model that enables the "on target-off tumor" assessment of TCBs in the presence of PBMCs under flow. Our model emulates the 3 dimensional microenvironment within human kidneys through the inclusion of podocyte-rich glomeruli, proximal and distal tubules, and microvasculature that comprise functional nephrons. Using two TCBs engineered to target peptide-HLA complexes with high (WT1-TCB*) or poor (ESK1-like TCB) specificity, we have shown that kidney organoids subjected to flow are sufficiently mature to exhibit WT1 expression in podocyte-rich clusters as well as upregulation of HLA-A2 via IFNγ stimulation. We further showed that in the absence of TCBs, PBMCs exhibit minimal alloreactivity against kidney organoids even though these cells are only partially HLA-A2 matched.

While cytotoxic T cell expansion and activation occur rapidly in our model, PBMCs require a few days to distribute throughout the kidney organoids (~100 mm thick). Although partial perfusion of their microvascular networks was previously reported (26), it is likely that PBMCs access these 3 dimensional organoid-based tissues via a combination of perfusion and cell migration. Even though an ideal model would enable their physiological delivery via controlled perfusion through the 3D kidney tissue, this current embodiment has utility for assessing TCB specificity using a combination of pharmacological readouts. Indeed, we find that WT1-TCB*-mediated cell killing is confined to $WT1^+$ cells, i.e., podocytes and $WT1^+LTL^+$ cells that reside in the transition zone (29, 30) between podocyte-rich clusters and proximal tubules. While flow enhances kidney organoid maturation, as reflected by selective WT1-TCB*-induced killing of podocytes, the podocyte-rich clusters lack a fully formed glomerular barrier (20, 29, 31). Given these deficiencies, it remains undetermined whether an intravenously administered TCB would reach WT1 expressing cells in human kidneys under physiological conditions leading to "on-target, off-tumor" effects. As further improvements in kidney organoid differentiation protocols emerge, we anticipate that such tissues will exhibit increasingly adult-like cell phenotypes and tissue microarchitectures (42).

In summary, by combining multicellular kidney organoid-on-chip technology with components of the immune system, we established an immune-infiltrated kidney organoid-on-chip model that provides a platform for studying on/off target effects of cancer therapeutics as well as immune cell interactions within healthy and diseased kidney tissues.

Materials and Methods

Kidney Organoid Differentiation. Kidney organoids are differentiated following the protocols reported by Morizane et al. (24, 25), with minor alterations for the stem cell maintenance culture: Briefly, H9 ESCs are maintained in mTeSR Plus (Stem Cell Technologies) on 1% Matrigel-coated (Stem Cell Technologies) treated tissue culture plastic. They are dissociated using Gentle Cell Dissociation Reagent (Stem Cell Technologies) and seeded at density of 18,000 cells/cm^2

in mTeSR Plus supplemented with 5 μM Y27632 (Tocris) and differentiated into nephron progenitor cells (NPCs) of the metanephric mesenchyme via a three-step differentiation protocol using 8 μM CHIR (Tocris), 10 ng/mL Activin A (R&D Systems), and 10 ng/mL Fibroblast Growth Factor 9 (FGF9, R&D Systems) sequentially over 8 d of culture in the differentiation medium Advanced RPMI (AdvRPMI, Thermo Fisher Scientific) supplemented with 1X GlutaMax (Thermo Fisher Scientific). On day 8, the NPCs are dissociated into single cells using a 15-min incubation with AccuMax (Stem Cell Technologies), counted, and seeded into AgreeWell800 6-well plates (Stem Cell Technologies) at an aggregate size of 10,000 cells/aggregate. The aggregation is performed in AdvRPMI with 1X GlutaMax, 10 ng/mL FGF9, and 3 μM CHIR. Then, 24 h post aggregation [day 8/9] depending on culture morphology as described in Morizane et al. (24)], the culture medium is changed to AdvRPMI with 1X GlutaMax with 10 ng/mL FGF9, and the aggregates are cultured in this medium for 72 h until day 11/12 of differentiation. Since not all seeded NPCs are participating in the aggregate, we assume that the final cell count per aggregate is ~8,000 cells. At day 12, they are either seeded onto an ECM (described below) for static culture or the same ECM housed in the millifluidic chip device (10).

ECM. A gelatin–fibrin matrix is produced using a previously reported method (26). Briefly, it is composed of 2 wt% (w/v) porcine gelatin type A (300 Bloom, Sigma), 10 mg/mL bovine fibrinogen (Millipore Sigma), and 2.5 mM Calcium chloride (Sigma), and cross-linked via a dual enzymatic cross-linking system that contains 0.2 wt% (w/v) transglutaminase (MooGloo, The Modernist Pantry), and 2 U/mL bovine thrombin (MP Biomedicals). Stock solutions of gelatin, fibrinogen, calcium chloride, and transglutaminase are prepared in the indicated concentrations in PBS without calcium and magnesium and incubated for 15 min at 37 °C. After this pre-cross-linking step, 1 mL of this stock solution is mixed with thrombin and quickly cast into the chip device until the ECM covers the entire glass surface inside the device or into a 35-mm Petri dish for static controls. The ECM is incubated for 3 h at 37 °C before seeding kidney organoids onto the surface of it.

Millifluidic Chips. Millifluidic chips are produced as reported previously (26). Briefly, polydimethylsiloxane (PDMS, SE1700, Dow Chemical) is 3D printed onto a 50- × 75-mm glass slide in the form of a gasket using a multimaterial 3D bioprinter equipped with four independently addressable printheads mounted onto a 3-axis, motion-controlled gantry with a build volume of 725 mm × 650 mm × 125 mm (AGB 10000, Aerotech Inc.). The PDMS ink is prepared at a ratio of 10:1 of base to cross-linker and mixed using a speed mixer (Flaktek), before loading it into a 35-cc syringe barrel (Nordson EFD) prior to printing. The printed gaskets were cured overnight at 80 °C.

The fully assembled chip consists of a printed silicone gasket that houses the cast and cross-linked ECM, which is placed onto a stainless-steel base, covered with a laser-cut acrylic lid (McMaster Carr), held in place by 4 screws (McMaster Carr). At the inlet port, a 1.25-mm OD stainless-steel pin is inserted and connected to the inlet tubing. The inlet tubing consists of a 10-cc syringe barrel fluid reservoir (Nordson EFD) with its lid, a luer lock nozzle, and a 1.85-mm inner diameter 2-stop tubing with adapter tubing to connect to the inlet pin. At the outlet port, another 1.25-mm OD stainless steel pin is insert and connected to the outlet tubing. The outlet tubing consists of clear silicone tubing and a stainless-steel pin that connects to the inlet fluid reservoir, closing the fluid circuit (Fig. 1). Both inlet and outlet tubing have clips to control fluid motion through the chip. All parts of the fully assembled device are autoclaved before use, apart from the tubing clips, acrylic lids, and 2-stop tubing, which are sterilized with 70% ethanol.

On day 11/12 of differentiation, the kidney organoids are seeded on the ECM within the millifluidic chips. The inlet tubing is assembled with a 0.2-μm polyether sulfone syringe filter in line, connected to the inlet pin at the inlet port of the printed gasket filled with ECM, which is placed onto the stainless-steel base. The outlet tubing is also connected. The chip gasket is filled with chip culture medium (AdvRPMI with 1X GlutaMax, 1.5% heat-inactivated fetal bovine serum, and 1% Antibiotic/Antimycotic solution) until the fluid covers ~3/4 of the surface of the ECM, and about 200 kidney organoids (~8,000 cells/organoid) are placed on the surface of the ECM. The organoids are allowed to settle onto the surface, the acrylic lid is carefully placed and screwed in place, and the chip is fully filled with fluid. After this kidney organoid seeding into the device, the chips are cultured at a flow rate of 42.5 μL/min (~0.0001 dyn/cm^2) by an 8-roller peristaltic pump (Ismatech) overnight to let the organoids adhere to the ECM. On day 12/13 of differentiation, the organoids are imaged using bright-field microscopy, the syringe filter is removed from the circuit and the flow rate is increased to 4.27 mL/min (0.008 to 0.035 dyn/cm^2). Culture medium is replaced every other day for the duration of culture. The chips are either cultured for 7 d (until day 18/19 of differentiation) at a flow rate of 4.27 mL/min and used in the T cell bispecific antibody–mediated killing assay or cultured for 10 d under flow (until day 21/22 of differentiation) and formaldehyde-fixed for immunofluorescence staining. For the low flow condition, the chips are kept at a flow rate of 42.5 μL/min.

TCB-Mediated Cell Killing Assay. All TCBs were purified from transiently transfected HEK293-EBNA or CHO cells via protein A affinity chromatography and size-exclusion chromatography, as previously reported (9). Affinities and avidities were characterized in surface plasmon resonance experiments using a Biacore T200. At day 19 of differentiation, after 7 d of culture on the flow, the TCB-mediated killing assay is initiated. Cryopreserved PBMCs (Cellero/Charles River Laboratories) are thawed in chip culture medium on the day of the assay according to the manufacturer's instructions. For these studies, four different PBMC donors are used (*SI Appendix*, Table S1). The inlet reservoir is replaced with a 3-cc fluid reservoir to minimize evaporation of culture medium during the assay. Before the assay is started, the chip culture medium (AdvRPMI with 1X GlutaMax, 1.5% fetal bovine serum, and 1% Antibiotic/Antimycotic solution) is replaced and the chip is filled with a final assay volume of 5.5 mL chip culture medium. The TCB is added in the appropriate concentration into the fluid reservoir and the PBMCs are seeded at 4 M cells/device by pipetting them directly into the chamber via the inlet port (effector to target cell ratio of 4:1). The PBMCs are allowed to settle onto the culture area where the kidney organoids are adherent, and the chips are left clipped in the incubator without flow for 30 min. After this, the flow is ramped to 3 mL/min over the course of 4 h. This is day 0 of the assay (Fig. 1). On day 1 and day 3, 250 μL of chip culture medium are sampled from the reservoir for analysis of LDH activity and cytokine profiling. All supernatants were centrifuged at 400 g to remove any cells and stored at −80 °C until they could be analyzed. On day 5, the chip is opened, and the chip culture medium, circulating and adherent PBMCs, and kidney organoids are collected in the same 15-mL falcon tube and spun down at 400 g. The supernatant is then analyzed to determine LDH activity and cytokine profile. The pellet is subsequently digested into single cells for flow cytometry staining in a two-step digestion protocol. To remove larger remnants of ECM, the pellet is first incubated for 3 min in 200 μL of 2.5% trypsin with EDTA (Thermo Fisher Scientific) and 10 mL of PBS without calcium or magnesium is added to dilute the trypsin solution. The sample is spun down again at 400 g and the supernatant is removed. Subsequently, the pellet is incubated for 15 to 20 min in 400 μL of 1 mg/mL collagenase IV (Stem Cell Technologies) and broken up into single by gentle pipetting with a P1000 and a P200 pipettor. When the cell solution does not contain visible aggregates anymore, 3.5 mL of PBS with calcium and magnesium is added and the resulting diluted cell solution is filtered through a 35 μm mesh cap into a flow cytometry tube for staining.

To determine flow effects on TCB-mediated cell killing, samples are cultured for 7 d under high or low flow and the killing assay was performed for the next 5 d under the same conditions. Samples are pooled for analysis depending on their flow condition during the 5-d killing assay.

For activation controls, PBMCs are seeded at 1 to 2 M cells into a 24-well plate and cultured with or without OKT3 (43) (Miltenyi Biotec) for the duration of the assay and subjected to the same digestion protocol for flow cytometry staining controls. To ensure robustness, the experiments in Figs. 1, 2, and 3 were performed with 2 different PBMC donors and 2 different batches of organoids, and the data presented were pooled.

Flow Cytometry. Single cell suspensions obtained from digested kidney organoids PBMCs are prepared for spectral cytometry analysis. Briefly, cells are first incubated with Yellow live/dead amine-reactive dye at 1:3,000 dilution (Thermo Fisher Scientific) for 20 min at room temperature in the dark. Cells are then washed in 1 mL of staining buffer containing 0.1% sodium azide and bovine serum albumin (BD Biosciences) and spun at 400 × g. To block nonspecific binding, cells are then incubated for 30 min at room temperature in the dark with anti-human FcR block (Mylteni) at 1:10 dilution. After blocking, cells are washed in staining buffer and incubated with cell surface–staining antibodies (*SI Appendix*, Table S2) for 30 min

at 4 °C in the dark (100 μL staining volume). Following antibody incubation, cells are washed twice in staining buffer then fixed for 20 min in 250 μL BD Cytofix (BD Biosciences) at room temperature in the dark. After fixing, cells are washed once more in staining buffer and resuspended in 100 μL of PBS. For characterization of intracellular markers, the cell membranes are permeabilized with 500 μL of 1X perm/wash buffer (Biolegend) for 30 min at room temperature in the dark. After permeabilization, cells are incubated for 30 min with intracellular staining antibodies (100 μL staining volume) at room temperature in the dark (*SI Appendix*, Table S2). For unconjugated antibodies, cells are further incubated for 1 h with a corresponding secondary antibody at room temperature in the dark (100 μL staining volume). Finally, cells are washed in 1 mL staining buffer and resuspended in 300 μL of PBS and counting beads (Thermo Fisher) are added for analysis in an Aurora spectral analyzer (CYTEK). Single color references and fluorescence minus one control are used in every experiment. For analysis, at least 250,000 events are collected. After acquisition, data are analyzed using FloJo™ software V.10 (BD Biosciences). The gating scheme is depicted in *SI Appendix*, Fig. S6*A*.

FLICA Staining. To visualize cell death, a fluorescent inhibitor probe is used, FAM-VAD-FMK, which labels active caspases intracellularly (Immunochemistry Technologies). Before fixation, the probe is incubated following the manufacturer's instructions for 2 h at a 1:150 dilution in serum-free chip culture medium at 37 °C in the incubator. Subsequently, the samples are washed three times for 10 min with 1X apoptosis buffer supplied by the manufacturer, and formaldehyde fixed (see below).

IFNγ Stimulation. To test their IFNγ response, kidney organoids are cultured on ECM under flow or static conditions (control) for 10 d (seeded on day 11/12 of differentiation) and then subjected to 500 U/mL IFNγ (Roche) (day 18/19 to day 21/22 of differentiation). After IFNγ exposure, the samples are either digested into single cells and stained for the appropriate marker for flow cytometry or formaldehyde-fixed for immunofluorescent staining and imaging.

Image Analysis. Since the kidney organoid size and seeding number vary between samples, we quantified the organoid area on Day 1 after seeding onto the ECM (day 13 of differentiation) for each sample and used these values for normalization. On day 13, bright-field microscopy images (Leica) are acquired across the entire area seeded with organoids on each chip. Images are stitched together using FIJI and pairwise stitching plugin (44). The images are analyzed in MATLAB (*SI Appendix*, Fig. S6*B*) as follows: The image is converted into a binary image based on its HSV values and inverted. The pixels around the organoids are dilated and eroded in two subsequent steps over two rounds and the area of white pixels is extracted. With the pixel size information from the microscope, the pixel area is converted into a value of mm^2, which is used to normalize the data acquired from the LDH activity and flow cytometry assays.

Immunofluorescent Staining. To prepare kidney organoids for immunofluorescent staining, samples are washed once with PBS with calcium and magnesium and then fixed in 10% formalin for 45 min. To remove the fixative, the organoids are washed three times in PBS with calcium and magnesium for 30 min, permeabilized, and blocked in 2% donkey serum (Sigma) and 0.125% Triton-X100 (Sigma) in PBS with calcium and magnesium overnight at 4 °C. Primary antibodies are incubated for 3 d at 4 °C in staining solution [0.125% Triton-X100 and 1% bovine serum albumin (Sigma) in PBS with calcium and magnesium] and washed out over the course of 8 h with three exchanges of PBS with calcium and magnesium. Secondary antibodies raised in donkey are incubated overnight at 4 °C in staining solution. Nuclear counterstaining is achieved by incubating the organoids with 1 μg/mL DAPI dihydrochloride in staining solution for 1 h. Secondary antibodies and DAPI are washed out over the course of 8 h with three exchanges of PBS with calcium and magnesium. The samples were imaged on a confocal laser scanning microscope (Zeiss) and processed in Fiji for maximum intensity projections and Imaris (Bitplane) for 3D reconstruction and rendering.

To visualize binding of the WT1-TCB*, kidney organoids cultured on static ECM for 10 d were incubated with 2 μg/mL of an AlexaFluor633 labeled WT1-TCB* (see below) in chip culture medium for 2 h at 37 °C in the incubator. The organoids were washed once with PBS with calcium and magnesium, fixed in formaldehyde (see above), subsequently counterstained for markers identifying the individual nephron structures. For live imaging and cell visualization within these tissues, PBMCs were labeled with the CellMask™ Green Plasma Membrane dye (Thermo Fisher) following the manufacturer's instructions and perfused through the chip. Prior to imaging, the chip was perfused with 2 mg/mL Ulex europaeus agglutinin labeled with TRITC for 30 min to counterstain the vasculature. The samples were washed once with medium and imaged on a laser scanning confocal microscope (Zeiss).

LDH Assay. The LDH assay is performed following the manufacturer's instructions (Promega). Briefly, the supernatants are thawed, and 50 μL of the sample is mixed with 50 μL assay buffer containing assay substrate and incubated in the dark at room temperature for 30 min to 2 h. Following the incubation, 50 μL of stop solution is added, and the absorption of the sample at 490 nm is read using a standard plate reader (BioTek).

Multiplexed Assay for Cytokine Profiling. Supernatants are collected, the cells are removed by centrifugation, and the remaining solutions are immediately frozen at −80 °C until measurement. Measurement of cytokines (Granzyme B, IFNγ, IL-2, IL-6, IL-8, IL-10, TNFα) is performed using customized Invitrogen ProcartaPlex multiplex immunoassays (reference PPX-07_MXFVK4Y, lot number 311354-000). Each kit contains a black 96-well plate (flat bottom plate), antibody-coated beads, detection antibody, streptavidin-R-phycoerythrin (SAPE), reading buffer, and universal assay buffer. In addition, standards with known concentration are also provided to prepare a standard curve (dilution factor 4 from Standard S1). According to the Invitrogen Publication Number MAN0024966 [Revision C0 (32)], the assay workflow is the following: After adding the beads into the flat bottom plate, the beads are washed using a flat magnet and an automated plate washer (405TS microplate washer from Bioteck). Standards and samples diluted with universal buffer are then added into the plate and a first incubation is started for 2 h. After a second wash, detection antibody is added. After 30 min of incubation and a wash, SAPE is added. Finally, after 30-min incubation and a last wash, the beads are resuspended in the reading buffer and are ready for analysis. The data are acquired with a Luminex™ instrument, BioPlex-200 system from Bio-Rad. Using the Certificate of Analysis provided with the kit, bead region and standard concentration value S1 for each analyte of the current lot are entered in the software, BioPlex Manager. Plotting the expected concentration of the standards against the mean fluorescent intensity generated by each standard, the software generates the best curve fit and calculates the concentrations of the unknown samples (in pg/mL) according to their dilution factor. The upper limit of quantification (ULOQ) and the lower limit of quantification (LLOQ) are calculated according to their values on the calibration curves and the used dilution factor. In case of out of range, cytokine data are rounded at the ULOQ or LLOQ. The data are then exported in Excel and analyzed by GraphPad Prism.

Statistical Analysis. All bar graphs and dot plots are expressed as mean ± SD. For fold change, the samples are normalized by the average of the no TCB control. Statistical analysis was done in GraphPad Prism and differences between samples were considered statistically significant with a *P*-value below 0.05 when running a one-way ANOVA with Tukey's post-test for multiple comparisons. Each data point represents measurements from a sample, technical replicates are not shown. For Figs. 2 and 3, the data shown are pooled from two different experiments with different kidney organoid batches as well as PBMC donors. For these experiments, the sample groups are run in quintuplicates. To ensure comparison between donors with varying activities used in the experiments, all data are normalized to the 0 μg/mL TCB condition, where kidney organoids are present on chip and PBMCs are seeded, but no TCB is added. Fig. 4 is data collected from a single PBMC donor experiment with samples run in quadruplicates. Chip devices were only excluded from analysis when their failure was significant, for example, they had cracked and leaked out.

The number of batches of organoids, biological replicates, and technical replicates used in this study are provided in *SI Appendix*, Table S3.

Data, Materials, and Software Availability. Data from this study are available on the Materials Data Facility at https://doi.org/10.18126/E8Y5-AYFT (45).

ACKNOWLEDGMENTS. We gratefully acknowledge the experimental assistance provided by Jenny Yao, who contributed to early efforts in organoid differentiation and image analysis, respectively, and by Szilvia Heja, Robert Barber, and Zach Niziolek. Furthermore, we thank Dr. Benjamin Humphreys

and his team for generously providing the scientific community with online tools to access single-cell and single-nuclei RNAseq datasets of healthy and diseased, human and mouse kidneys, as well as organoids derived from various protocols. This open-access software platform (http://humphreyslab.com/SingleCell/) has aided in confirming gene expression data of WT1. We thank Drs. Navin Gupta, and Sebastien Uzel for useful discussions. This work was supported by the Roche Pharma Research & Early Development, Roche Innovation Center Basel, NIH National Center for Advancing Translational 621 Sciences (NCATS) through NIH UH3 Grant TR002155 (J.A.L., M.M.M., and R.M.), and International Foundation of Ethical Research Research Fellowship (awarded to K.T.K.).

Author affiliations: [a]Harvard University, School of Engineering and Applied Sciences, Cambridge, MA 02138; [b]Wyss Institute for Biologically Inspired Engineering, Boston, MA 02115; [c]Complex in vitro Systems, Safety Assessment, Genentech Inc., South San Francisco, CA 94080; [d]Roche Pharma Research and Early Development, Roche Innovation Center Basel, Basel CH-4070, Switzerland; [e]Roche Pharma Research and Early Development, Roche Innovation Center Munich, Munich DE-82377, Germany; [f]Department of Medicine, Harvard Medical School, Boston, MA 02115; and [g]Harvard Stem Cell Institute, Cambridge, MA 02138

Author contributions: K.T.K., K.A.H., A.M., M.G., A.-C.W., E.M.-B., and J.A.L. designed research; K.T.K., M.M.M., K.A.H., V.M., A.C., and K.H. performed research; K.T.K., M.M.M., and V.M. analyzed data; K.A.H. reviewed the paper drafts; R.M. edited the manuscript and supervised K.H.; A.M., E.M.-B. and A.-C.W. edited the manuscript; and K.T.K., M.M.M., and J.A.L. wrote the paper.

Reviewers: P.L., Eberhard Karls University Tübingen; and K.M., Cincinnati Children's Hospital and Medical Center Hospital Medicine.

1. M. E. Goebeler, R. C. Bargou, T cell-engaging therapies–BiTEs and beyond. *Nat. Rev. Clin. Oncol.* **17**, 418–434 (2020), 10.1038/s41571-020-0347-5.
2. C. Rosenfeld, M. A. Cheever, A. Gaiger, WT1 in acute leukemia, chronic myelogenous leukemia and myelodysplastic syndrome: Therapeutic potential of WT1 targeted therapies. *Leukemia* **17**, 1301–1312 (2003), 10.1038/sj.leu.2402988.
3. T. Dao *et al.*, Targeting the intracellular WT1 oncogene product with a therapeutic human antibody. *Sci. Transl. Med.* **5**, 176ra33 (2013).
4. T. Dao *et al.*, Therapeutic bispecific T-cell engager antibody targeting the intracellular oncoprotein WT1. *Nat. Biotechnol.* **33**, 1079–1086 (2015).
5. "The Wilms' Tumor (WT1)" in *Gene Methods and Protocols*, N. Hastie Ed. (Springer Science+Business Media, New York, NY, USA, 2016), vol. **1467**, p. 235.
6. N. Daver, A. S. Alotaibi, V. Bücklein, M. Subklewe, T-cell-based immunotherapy of acute myeloid leukemia: Current concepts and future developments. *Leukemia* **35**, 1843–1863 (2021), 10.1038/s41375-021-01253-x.
7. A. Viardot, R. Bargou, Bispecific antibodies in haematological malignancies. *Cancer Treat. Rev.* **65**, 87–95 (2018), 10.1016/j.ctrv.2018.04.002.
8. N. Veomett *et al.*, Therapeutic efficacy of an Fc-enhanced TCR-like antibody to the intracellular WT1 oncoprotein. *Clin. Cancer Res.* **20**, 4036–4046 (2014).
9. C. Augsberger *et al.*, Targeting intracellular WT1 in AML with a novel RMF-peptide-MHC-specific T-cell bispecific antibody. *Blood* **138**, 2655–2669 (2021).
10. S. Rafiq *et al.*, Optimized T-cell receptor-mimic chimeric antigen receptor T cells directed toward the intracellular Wilms Tumor 1 antigen. *Leukemia* **31**, 1788–1797 (2017).
11. Y. Y. Chau, N. D. Hastie, The role of Wt1 in regulating mesenchyme in cancer, development, and tissue homeostasis. *Trend Genet.* **28**, 515–524 (2012), 10.1016/j.tig.2012.04.004.
12. L. Yin, X.-J. Wang, D.-X. Chen, X.-N. Liu, X.-J. Wang, Humanized mouse model: A review on preclinical applications for cancer immunotherapy. *Am. J. Cancer Res.* **10**, 4568–4584 (2020).
13. P. Kubiniok *et al.*, Understanding the constitutive presentation of MHC class I immunopeptidomes in primary tissues. *iScience* **25**, 103768 (2022).
14. E. Marrer-Berger *et al.*, Genome sequencing analysis identifies high-risk Epstein-Barr virus subtypes for nasopharyngeal carcinoma. Research Square [Preprint] (2022). https://doi.org/10.21203/rs.3.rs-1828302/v1 (Accessed 20 July 2022).
15. D. E. Ingber, Human organs-on-chips for disease modelling, drug development and personalized medicine. *Nat. Rev. Genetics* **23**, 467–491 (2022), 10.1038/s41576-022-00466-9.
16. S. N. Bhatia, D. E. Ingber, Microfluidic organs-on-chips. *Nat. Biotechnol.* **32**, 760–772 (2014).
17. S. Musah *et al.*, Mature induced-pluripotent-stem-cell-derived human podocytes reconstitute kidney glomerular-capillary-wall function on a chip. *Nat. Biomed. Eng.* **1**, 0069 (2017).
18. K. Doi *et al.*, Enhanced podocyte differentiation and changing drug toxicity sensitivity through pressure-controlled mechanical filtration stress on a glomerulus-on-a-chip. *Lab Chip* **23**, 437–450 (2023), 10.1039/d2lc00941b.
19. M. H. Little, Growing kidney tissue from stem cells: How far from "party trick" to medical application? *Cell Stem Cell* **18**, 695–698 (2016).
20. M. H. Little, A. N. Combes, Kidney organoids: Accurate models or fortunate accidents. *Genes Dev.* **33**, 1319–1345 (2019).
21. J. Y. C. Soo, J. Jansen, R. Masereeuw, M. H. Little, Advances in predictive in vitro models of drug-induced nephrotoxicity. *Nat. Rev. Nephrol.* **14**, 378–393 (2018), 10.1038/s41581-018-0003-9.
22. L. M. A. Barnett, B. S. Cummings, Nephrotoxicity and renal pathophysiology: A contemporary perspective. *Toxicol. Sci.* **164**, 379–390 (2018).
23. H. Y. Tiong *et al.*, Drug-induced nephrotoxicity: Clinical impact and preclinical in vitro models. *Mol. Pharm.* **11**, 1933–1948 (2014).
24. R. Morizane, J. V. Bonventre, Generation of nephron progenitor cells and kidney organoids from human pluripotent stem cells. *Nat. Protoc.* **12**, 195–207 (2017).
25. R. Morizane *et al.*, Nephron organoids derived from human pluripotent stem cells model kidney development and injury. *Nat. Biotechnol.* **33**, 1193–1200 (2015).
26. K. A. Homan *et al.*, Flow-enhanced vascularization and maturation of kidney organoids in vitro. *Nat. Methods* **16**, 255–262 (2019).
27. R. S. Gejman *et al.*, Identification of the targets of T-cell receptor therapeutic agents and cells by use of a high-throughput genetic platform. *Cancer Immunol. Res.* **8**, 672–684 (2020).
28. U. Boehm, T. Klamp, M. Groot, J. C. Howard, Cellular responses to Interferon-**γ**. *Annu. Rev. Immunol.* **15**, 749–795 (1997).
29. H. Wu *et al.*, Comparative analysis and refinement of human PSC-derived kidney organoid differentiation with single-cell transcriptomics. *Cell Stem Cell* **23**, 869–881.e8 (2018).
30. H. Wu *et al.*, Single-cell transcriptomics of a human kidney allograft biopsy specimen defines a diverse inflammatory response. *J. Am. Soc. Nephrol.* **29**, 2069–2080 (2018).
31. H. Wu, B. D. Humphreys, Single cell sequencing and kidney organoids generated from pluripotent stem cells. *Clin. J. Am. Soc. Nephrol.* **15**, 550–556 (2020).
32. D. Cibrián, F. Sánchez-Madrid, CD69: From activation marker to metabolic gatekeeper. *Eur. J. Immunol.* **47**, 946–953 (2017), 10.1002/eji.201646837.
33. D. A. Walsh *et al.*, The functional requirement for CD69 in establishment of resident memory CD8 + T cells varies with tissue location. *J. Immunol.* **203**, 946–955 (2019).
34. S. Létourneau, C. Krieg, G. Pantaleo, O. Boyman, IL-2- and CD25-dependent immunoregulatory mechanisms in the homeostasis of T-cell subsets. *J. Allergy Clin. Immunol.* **123**, 758–762 (2009).
35. M. Kmieciak *et al.*, Human T cells express CD25 and Foxp3 upon activation and exhibit effector/memory phenotypes without any regulatory/suppressor function. *J. Transl. Med.* **7**, 89 (2009).
36. J. F. Viallard *et al.*, CD8+HLA-DR+ T lymphocytes are increased in common variable immunodeficiency patients with impaired memory B-cell differentiation. *Clin. Immunol.* **119**, 51–58 (2006).
37. J. M. Hope *et al.*, Fluid shear stress enhances T cell activation through Piezo1. *BMC Biol.* **20**, 61 (2022).
38. C. S. C. Liu *et al.*, Cutting edge: Piezo1 mechanosensors optimize human T cell activation. *J. Immunol.* **200**, 1255–1260 (2018).
39. A. Jaigirdar, S. A. Rosenberg, M. Parkhurst, A high-avidity WT1-reactive T-cell receptor mediates recognition of peptide and processed antigen but not naturally occurring WT1-positive tumor cells. *J. Immunother.* **39**, 105–116 (2016).
40. C. J. Holland *et al.*, Specificity of bispecific T cell receptors and antibodies targeting peptide-HLA. *J. Clin. Invest.* **130**, 2673–2688 (2020).
41. S. J. Kerns *et al.*, Human immunocompetent organ-on-chip platforms allow safety profiling of tumor-targeted t-cell bispecific antibodies. *Elife* **10**, e67106 (2021).
42. K. J. Wolf, J. D. Weiss, S. G. M. Uzel, M. A. Skylar-Scott, J. A. Lewis, Biomanufacturing human tissues via organ building blocks. *Cell Stem Cell* **29**, 667–677 (2022).
43. U. Landegren, J. Andersson, H. Wigzell, Mechanism of T lymphocyte activation by OKT3 antibodies. A general model for T cell induction. *Eur. J. Immunol.* **14**, 325–328 (1984).
44. S. Preibisch, S. Saalfeld, P. Tomancak, Globally optimal stitching of tiled 3D microscopic image acquisitions. *Bioinformatics* **25**, 1463–1465 (2009).
45. K. T., Kroll *et al.*, Dataset for Kroll, Mata, Homan et al. 'Immune-infiltrated Kidney Organoid-on-Chip Model for Assessing T Cell Bispecific Antibodies', PNAS, 2023. Materials Data Facility. https://doi.org/10.18126/E8Y5-AYFT. Deposited 24 July 2023.